Clim Dyn
DOI 10.1007/s00382-009-0666-9

Influence of ENSO and the South Atlantic Ocean on climate predictability over Southeastern South America

Marcelo Barreiro

Received: 2 April 2009 / Accepted: 10 September 2009

Abstract We perform a systematic study of the predictability of surface air temperature and precipitation in Southeastern South America (SESA) using ensembles of AGCM simulations, focusing on the role of the South Atlantic and its interaction with the El Niño-Southern Oscillation (ENSO). It is found that the interannual predictability of climate over SESA is strongly tied to ENSO showing high predictability during the seasons and periods when there is ENSO influence. The most robust ENSO signal during the whole period of study (1949–2006) is during spring when warm events tend to increase the precipitation over Southeastern South America. Moreover, the predictability shows large inter-decadal changes: for the period 1949–1977, the surface temperature shows high predictability during late fall and early winter. On the other hand, for the period 1978–2006, the temperature shows (low) predictability only during winter, while the precipitation shows not only high predictability in spring but also in fall. Furthermore, it is found that the Atlantic does not directly affect the climate over SESA. However, the experiments where air–sea coupling is allowed in the south Atlantic suggest that this ocean can act as a moderator of the ENSO influence. During warm ENSO events the ocean off Brazil and Uruguay tends to warm up through changes in the atmospheric heat fluxes, altering the atmospheric anomalies and the predictability of climate over SESA. The main effect of the air–sea coupling is to strengthen the surface temperature anomalies over SESA; changes in precipitation are more subtle. We further found that the thermodynamic coupling can increase or decrease the predictability. For example, the air–sea coupling significantly increases the skill of the model in simulating the surface air temperature anomalies for most seasons during period 1949–1977, but tends to decrease the skill in late fall during period 1978–2006. This decrease in skill during late fall in 1978–2006 is found to be due to a wrong simulation of the remote ENSO signal that is further intensified by the local air–sea coupling in the south Atlantic. Thus, our results suggest that climate models used for seasonal prediction should simulate correctly not only the remote ENSO signal, but also the local air–sea thermodynamic coupling.

Keywords ENSO · South Atlantic · Climate predictability · Southeastern South America · Thermodynamic air–sea interaction

M. Barreiro (✉)
Unidad de Ciencias de la Atmósfera, Instituto de Física, Facultad de Ciencias, Universidad de la República, Igua 4225, 11100 Montevideo, Uruguay
e-mail: barreiro@fisica.edu.uy

1 Introduction

Climate variability in Southeastern South America (SESA, here defined as the continental region within [65°W–47°W, 19°S–37°S]) is influenced by the El Niño-Southern Oscillation (ENSO) as well as by internal atmospheric dynamics (e.g., Ropelewski and Halpert, 1987, 1989; Grimm et al. 2000). While the latter can not be predicted beyond the 1–2 week limit determined by chaotic dynamics, the former enhances the predictability of climate in the region due to the slower evolution of the ocean. In fact, most of the seasonal predictions made for the region consider mainly the state of the tropical Pacific as a predictor. The recent studies by Nobre et al. (2004, 2006) summarize the effects of ENSO over SESA; here we only mention the main relevant results.

Published online: 22 September 2009

In the case of precipitation the most robust signal occurs during the spring and consists of enhanced (reduced) rainfall over SESA during a warm (cold) ENSO event (we consider southern hemisphere seasons). The mechanisms through which El Niño influences SESA involve both upper and lower level atmospheric circulation anomalies. During El Niño the strengthening and meandering of the subtropical jet in upper levels due to Rossby wave trains propagating from the equatorial Pacific increases baroclinicity and the advection of cyclonic vorticity over SESA (Yulaeva and Wallace 1994; Grimm et al. 2000). In lower levels the northerly flow from the Amazon basin strengthens increasing the availability of moisture south of 20°S (Silvestri 2004). During high summer the subtropical jet moves poleward weakening the upper level mechanism and the signal weakens. In later summer the signal strengthens again, and if only El Niño events that last until the following May are considered, there is a significant positive anomaly in the region during fall that induces floods of the Parana river (Camilloni and Barros 2003).

The ENSO influence on surface temperature has drawn much less attention. Among the few studies, the observational analysis of Kiladis and Diaz (1989) shows that there is a tendency for above (below) normal temperatures in the region during warm (cold) events in winter. This was later confirmed by Barros et al. (2002), who found warm (cold) temperature anomalies in subtropical South America during the winter of the developing phase of El Niño (La Niña) due to enhanced (weakened) northerly flow. These authors further argue that the modest ENSO signal on surface temperature is due to the partial balance between the effects of advection of heat and moisture due to a modified northerly flow. The exception is during winter when precipitation (which leads to local cooling due to cloudiness and evaporation) over subtropical South America is not related to an anomalous northerly flow.

Nobre et al. (2004) stress the large inter-event variability of the ENSO signal over SESA. Possible causes proposed to explain this inter-event variability are the strength of El Niño (Silvestri 2004), the state of the subtropical south-central Pacific (Barros and Silvestri 2002), and the effect of the equatorial Atlantic (Barreiro and Tippmann 2008). Another possibility are changes in the ENSO evolution. Wang (1995) showed that the evolution of ENSO has changed since mid-1970s: while before the SST anomaly started in the eastern coast and developed westward, after mid-1970s the initial SST anomaly appears in the central Pacific and migrates toward the eastern boundary. Moreover, most of El Niño events that lasted until the fall of the year following the onset occurred after mid-1970s. These changes in ENSO evolution likely affected the climate teleconnections and their impact on SESA. For example, Antico (2008) found that the persistence of ENSO SST anomaly after the 1970s induces increased precipitation in the fall following the peak of the event.

Recently, it has been reported that the tropical Indian Ocean can affect rainfall and temperatures over South America during spring. Accordingly, a positive Indian Ocean Dipole event induces positive temperature and rainfall anomalies over SESA (Saji et al. 2005; Chan et al. 2008). Both studies find that the connection is done through a Rossby-wave train that extends from the Indian Ocean to the subtropical south Atlantic.

On the other hand, the impact of the neighboring South Atlantic Ocean on SESA is not yet fully understood, even though some studies have presented evidence of a possible link. Moreover, most of the studies consider only the impact of this ocean basin on rainfall anomalies. For example, Diaz et al. (1998) found a connection between increased rainfall anomalies over SESA and warm SST anomalies off southern Brazil and the equatorial Atlantic during late spring and early summer. However, the simultaneous correlation is not indicative of a causal relationship, and both anomalies may be forced by another phenomenon (e.g., ENSO). Using AGCM simulations forced with prescribed patters of south Atlantic SST anomalies Robertson et al. (2003) found a very weak response of precipitation and surface temperature over SESA.

It has been show that the summertime climate in SESA is connected to the behavior of the South Atlantic Convergence Zone (SACZ) in the form of a rainfall seesaw: increased rains in the SACZ are correlated with decreased rainfall in SESA (Doyle and Barros 2002). The SACZ, in turn, may be forced by south Atlantic SST anomalies (Barreiro et al. 2002, 2005), but the main relationship seems to be that of an enhanced SACZ forcing a cold SST anomaly below and this in turn influences the convective activity there (Chaves and Nobre 2004; Robertson and Mechoso 2000). This is consistent with the study of Vianna Cuadra and Porfirio Da Rocha (2007) who found that the use of persisted SST in the south Atlantic has a very small impact on the summer climate over SESA simulated by a regional climate model.

Taschetto and Wainer (2008) studied the reproducibility of precipitation over South America due to south Atlantic SST in the context of a particular AGCM. Overall, they found large reproducibility (and thus predictability) in the tropical region, but very low in Southeastern South America, with a weak maximum in fall.

Finally, the south Atlantic is not independent of ENSO. Alexander et al. (2002) have shown that the south Atlantic tends to warm (cool) during El Niño (La Niña) events. Though they do not focus on this region they are able to simulate the observed warming using an AGCM coupled to a mixed layer ocean, suggesting that SST anomalies are

created mainly by anomalous heat fluxes. The mechanism involved in this connection is not clear. One candidate is the tropical troposphere temperature mechanism proposed by Chiang and Sobel (2002). In this mechanism the remote surface temperature warming is seen as the adjustment of the remote tropical oceans to the tropospheric temperature increase that occurs during El Niño. The connection to the surface is done through moist convection which increases the moist static energy in the boundary layer, decreasing the latent heat flux and warming the surface ocean.

Most of the above studies are concerned with a particular season, and/or focus only on precipitation or temperature. Here we investigate systematically the predictability of surface air temperature and precipitation over SESA for all seasons using an AGCM forced with historical SST and coupled to a slab ocean in the south Atlantic. We focus on the role of the south Atlantic as directly forcing climate anomalies, as well as on the possibility that it acts as a moderator of external influences, e.g., from ENSO. We pay special attention to the relationship between SST in the south Atlantic and surface temperature anomalies over SESA, that has not yet been studied in detail. Moreover, we study the inter-decadal variations in predictability by comparing the periods 1949–1977 and 1978–2006. Results show that the predictability of the region is largely due to ENSO, and that it shows large inter-decadal changes due to changes in the ENSO remote influence. Moreover, we found that even though the south Atlantic does not directly influence climate over SESA, its response to ENSO can modify the direct ENSO signal over SESA, altering the climate predictability in the region.

2 Model and experiments

We use Speedy, a full atmospheric general circulation model (AGCM) with simplified physics and an horizontal resolution of T30 (3.75° × 3.75°) with 8 vertical levels (Molteni 2003; Kucharski et al. 2005).

Speedy is run in two modes: as a stand-alone AGCM forced with imposed historical SST, and coupled to an oceanic slab ocean of fixed 50 m depth in the south Atlantic. In order to simulate the climatological SST reasonably well, the slab ocean needs a Q-flux that represents the climatological ocean heat transport. This Q-flux is calculated using the net surface heat flux of an experiment where the AGCM is forced with prescribed climatological SST. This simple ocean model captures the thermodynamic interaction between the ocean and the atmosphere, and the SST anomalies are generated only through changes in the atmospheric fluxes of heat.

Table 1 describes the main experiments. The model was forced with the Extended Reconstructed Sea Surface Temperature data set version 2 (ERSSTv.2, Smith and Reynolds 2004), and there is a linear blend between regions where SST is imposed/calculated differently.

The GOGA experiment gives a measure of climate predictability if the global SST were known perfectly in advance, while AOGA measures the direct influence of the tropical and south Atlantic basins. The comparison between GOGA-SACL and GOGA-SAML (which allows thermodynamic air–sea interaction in the south Atlantic) measures the importance of the response of the south Atlantic to remote forcings in the predictability of climate over SESA. Finally, the comparison among GOGA, GOGA-SACL and GOGA-SAML allows to isolate the effect of not knowing in advance the SST in the south Atlantic while knowing the SST elsewhere.

We consider the period 1949–2006, and constructed a 10-member ensemble for each experiment. The predictability measure used in this study is the correlation between the rainfall or temperature anomalies of the ensemble mean of each experiment and the corresponding observed quantity. This is calculated for the 12 running trimesters

Table 1 Experiments performed with the Speedy atmospheric general circulation model. Each experiment consists of a 10-member ensemble of integrations started from different initial conditions

Name of the experiment	Description
GOGA	Speedy forced with global historical SST everywhere
AOGA	Speedy forced with historical SST in the Atlantic between 50°S and 30°N and climatological SST everywhere else
GOGA-SACL	Speedy forced with historical SST everywhere except in the south Atlantic between 50°S and 10°S where climatological SST are imposed
GOGA-SAML	Speedy forced with historical SST everywhere except in the south Atlantic between 50°S and 10°S where the AGCM is coupled to a 50 m deep slab ocean
GOGA-SAML-NOC	Speedy forced with historical SST everywhere except in the south Atlantic where the ensemble mean SST of the GOGA-SAML experiment are imposed

(JFM,FMA,…,DJF). We also perform linear regression analysis to determine the pattern of climate anomalies.

As observations we use the surface air temperature field from the NCEP-NCAR Reanalysis CDAS-1 (originally on a 2.5° × 2.5° grid, Kalnay et al. 1996) interpolated onto the same horizontal grid as the Speedy model. Note that by surface air temperature we mean the air temperature at 1,000 hPa. This choice, instead of the usual 2 m temperature, was due to the low resolution of Speedy which has the lowest model level at $\sigma = 0.95$ (925 hPa). The model extrapolates the temperature to $\sigma = 1$ using the two lowest levels in order to calculate the near-surface air temperature for surface flux calculations (Speedy manual, available at http://users.ictp.it/~kucharsk/speedy_description/km_ver40_appendixA.pdf). We thus decided to use the model temperature at $\sigma = 1$ to compare to the Reanalysis temperature at 1,000 hPa.

For observed precipitation over land we use the PREC-L data set of Chen et al. (2002). This rainfall product is based on gauge observations from the Global Historical Climate Network, regridded on a 2.5° × 2.5° grid.

The GOGA experiment represents the observed annual cycle of interannual standard deviation of surface temperature over SESA very well (upper panel, Fig. 1). As in observations it has a maximum of about 0.9°C in winter, and a minimum of about 0.4°C during summer. On the other hand, the simulation of precipitation over SESA presents biases. While the model represents satisfactorily the climatological rainfall in the second half of the year, it rains about half that observed during the first half (middle panel, Fig. 1). This bias is also reflected in the standard deviation of interannual anomalies: while observed precipitation has maximum interannual variability during early fall and late spring, Speedy has maximum variability in spring and misses the early fall maximum (lower panel, Fig. 1). Spatially, the model has a bias consisting in a rainfall maximum in the western part of SESA, instead of a more uniform observed rainfall distribution (Kucharski et al. 2005). This bias is also found in the anomalies. For example, during El Niño years the simulated anomalies are located in the northwestern part of SESA, instead of in a more central location.

The ensemble mean of GOGA has similar annual cycles of interannual standard deviation for temperature and precipitation over SESA but with the amplitudes reduced to an average of about 50% of its value in the ensemble members (Fig. 1), showing that a significant part of rainfall and temperature anomalies is forced by SST, and suggesting the existence of predictability.

In order to study the inter-decadal variability we divided the whole period into two equally long subperiods: 1949–1977 (hereafter PERIOD1) and 1978–2006 (hereafter PERIOD2). The break between periods coincides with the

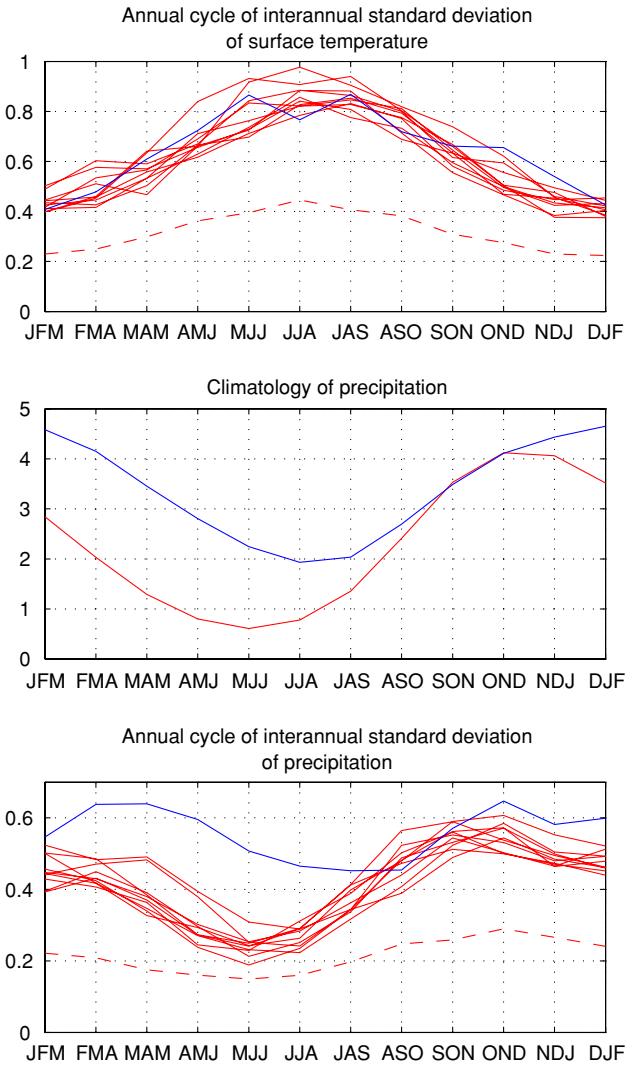

Fig. 1 *Upper panel*: Annual cycle of interannual standard deviation of surface temperature (K) over SESA for ensemble members of GOGA (*solid red*), ensemble mean of GOGA (*dashed red*), and observations (*blue*). *Middle panel*: Climatology of precipitation (mm day^{-1}) for observations (*blue*) and GOGA (*red*). *Lower panel*: same as upper panel but for precipitation (mm day^{-1})

"climate shift" of the mid-1970s, allowing to study the effect of changes in the ENSO evolution on the climate over SESA.

3 Surface air temperature

3.1 Predictability

Figure 2 shows the correlation between the ensemble mean surface air temperature of each experiment and the observed temperature over SESA for each trimester. It is easily seen that there are large differences in predictability between the two periods (compare the panels of Fig. 2):

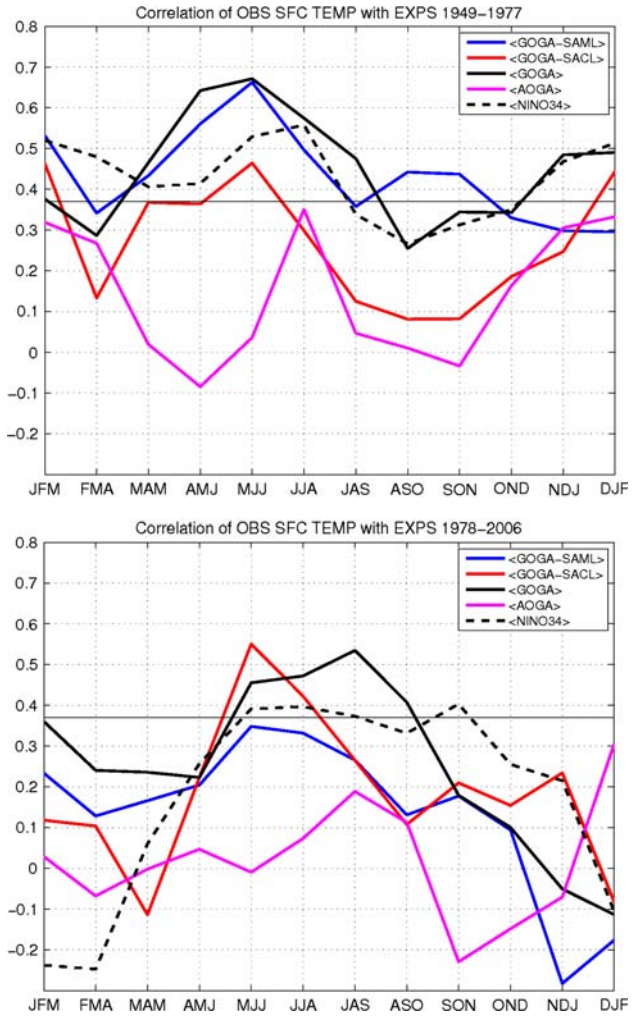

Fig. 2 Predictability of temperature over SESA as measured by the linear correlation between the observations and the ensemble mean of each experiment (*solid lines*). The key for the experiments is shown in the upper right corner. The *dashed black line* is the correlation between observed temperature over SESA and the simultaneous Niño3.4 index. The *horizontal line* marks the values significant at 5% level using a 2-sided student *t* test. *Upper panel* shows for period 1949–1977, and *lower panel* for period 1978–2006

while in PERIOD1 the correlation skill of the GOGA experiment is significant during several seasons, during PERIOD2 the skill is only significant in winter, and relatively low.

A second clear result is the lack of skill of the model to represent the interannual variability of temperature over SESA when only Atlantic SST anomalies are used. For the AOGA experiment, the correlations are very low and never statistically significant (both panels of Fig. 2). Thus, according to this model, the Atlantic basin does not force directly surface air temperature anomalies over SESA. As a consequence, the predictability of the GOGA experiment must arise due to the influence of the (tropical) Pacific and/or Indian Oceans, two oceans that are tightly coupled through atmospheric and oceanic bridges. From both panels of Fig. 2 it is seen that the correlation skill of GOGA follows a similar behavior as the correlation between the observed surface air temperature and the simultaneous Niño3.4 index (average of SST anomaly within [5°S–5°N, 170°W–120°W]). Thus, the predictability of GOGA seems to arise mainly due to the forcing from the tropical Pacific, agreeing with the literature (see also below). This is also supported by the similar behavior of GOGA's skill in simulating rainfall and the correlation between Niño3.4 and observed rainfall over SESA in Fig. 10.

To test the dependence of the relationship between observed anomalies over SESA and ENSO we calculated the correlation between precipitation/temperature and the Multivariate ENSO Index (available at http://www.cdc.noaa.gov/people/klaus.wolter/MEI/mei.html, Wolter and Timlin 1993, 1998). As shown in Fig. 3, the correlation between MEI and climate anomalies over SESA follows the same behavior as seen for Niño3.4 in Figs. 2 and 10. There are some changes in the magnitudes of the correlation values, e.g., in PERIOD1 during MJJ season MEI shows a correlation with temperature larger than 0.6, while Niño3.4 shows a correlation close to 0.53. Nevertheless, it is clear that the overall behavior is independent of the index used to describe ENSO.

One caveat to the above conclusion is the documented influence of the Indian Ocean during spring mentioned in the introduction. An additional (10 member) experiment forcing the AGCM only with Indian Ocean SST anomalies shows that the model captures the influence of this ocean basin over SESA during spring, while it has no skill in other seasons. However, the spring influence is weak and occurs mainly during 1949–1977. Since spring is not the focus of this study, we will not pursue this result here. Thus, from now on we will neglect the small contribution from the Indian Ocean during spring, and will consider that to first order the predictability of GOGA comes mainly from the tropical Pacific.

It is important to stress that, as expected, GOGA has the largest predictability of all experiments for most of the year because the SST are known perfectly in advance. Exceptions occur during PERIOD1 in JFM and late winter-early spring when GOGA-SAML shows higher predictability than GOGA, suggesting that air–sea interaction plays an important role in these seasons and the prescription of SST leads to a decrease in skill. This supports the use of forecast systems for seasonal prediction that take into account air–sea coupling in this region, with the caveat that the effect of air–sea interaction seems to depend on the period considered (compare PERIOD1 and PERIOD2).

Calculating the predictability for individual months suggests that the high predictability of GOGA-SAML during JFM is mainly because of an improved correlation

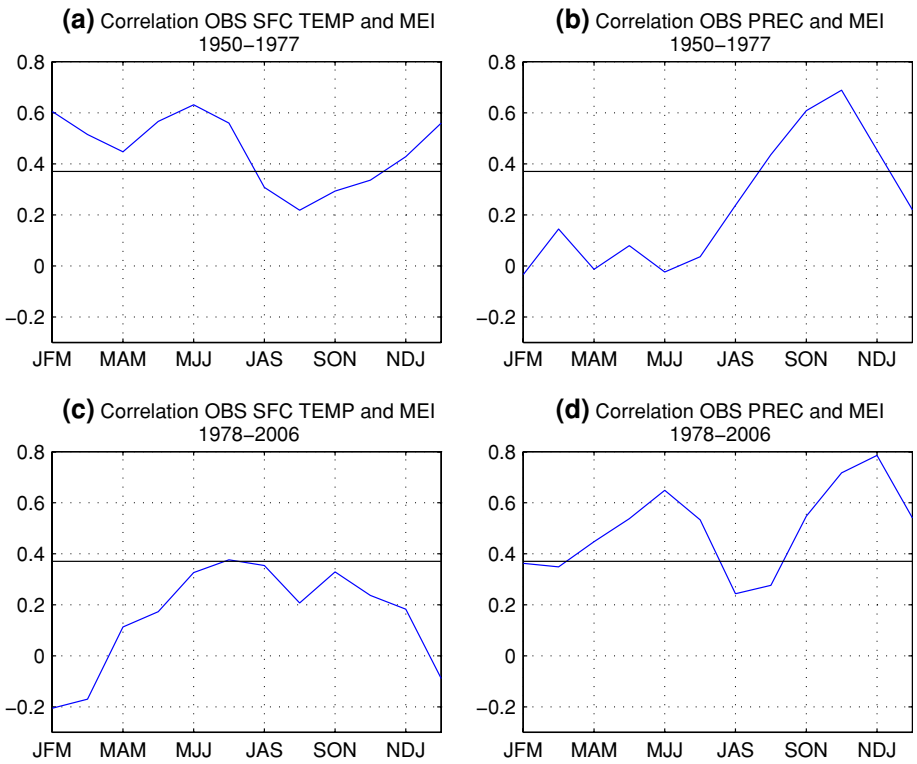

Fig. 3 Correlation between observed anomalies over SESA and the Multivariate ENSO Index (MEI) during PERIOD1 for (**a**) temperature and (**b**) precipitation, and during PERIOD2 for (**c**) temperature and (**d**) precipitation. Note that since the MEI starts in 1950, the correlation in PERIOD1 is calculated using years between 1950 and 1977

during March. Moreover, for March the use of a slab ocean increases to 5 months the persistence of temperature anomalies over SESA, the longest in the first half of the year (not shown). Thus, we speculate that during March the air–sea thermodynamic interaction off Brazil is particularly important in maintaining the persistence of the atmospheric anomalies induced by a relatively strong ENSO influence, making the evolution of anomalies closer to observations.

An additional interesting result that also hints a role for the south Atlantic SST is the difference between the skill of the model with climatological SST in the south Atlantic versus the case where the model is coupled to a slab ocean in that region (upper panel, Fig. 2). During PERIOD1 (1949–1977) the predictability of the experiment GOGA-SAML is significantly larger than that of GOGA-SACL for almost all year long. While for GOGA-SACL the correlation is barely significant, the correlation skill of GOGA-SAML is comparable to that of GOGA during late fall and early winter. This implies that the air–sea thermodynamic interaction in the south Atlantic can modify the atmospheric anomalies and change the climate predictability over SESA. This is discussed in more detail in Sect. 4.

In PERIOD2 (1978–2006) the predictability of temperature decreases significantly during the whole year (lower panel of Fig. 2). Moreover, the high skill found in late fall during PERIOD1 disappears, and the highest predictability is now in the middle of winter. The late spring-early summer predictability maximum of PERIOD1 is also absent. This behavior can be traced back to the change in the influence of ENSO over SESA illustrated by the correlation between observed temperature and the Niño3.4 index. In this latter period ENSO did not influence the surface temperature over SESA significantly, except—and weakly—for the winter season. Thus, in PERIOD2 surface temperature over SESA was mainly influenced by atmospheric internal variability, resulting in a low predictability.

Overall, the above results suggest that ENSO has a significant, but not very strong, influence on temperature over SESA in wintertime (JJA-JAS) during the whole period of study, in agreement with Kiladis and Diaz (1989) and Barros et al. (2002). The ENSO influence in other seasons, and thus the predictability of surface temperature, presents large interdecadal fluctuations.

3.2 Fall season

Late fall (MJJ) is the season that shows the largest changes in predictability before and after the mid-1970s, and one for which the use of a slab ocean in the south Atlantic seems to play an important role (compare GOGA-SACL and GOGA-SAML). For example, while in PERIOD1 the thermodynamic interaction increased the predictability, in PERIOD2 it reduced the predictability of surface temperature. Moreover, since fall is the transition season of ENSO, the reported changes in its evolution (e.g., Wang 1995) likely affected the climate teleconnections. We now focus

on this season to further understand the processes that lead to the simulated predictability.

We first determine the region of the south Atlantic that plays a role in increasing the predictability of temperature during PERIOD1. To do so we regress global SST anomalies onto the average temperature anomalies over SESA during MJJ (Fig. 4). As expected, the map shows a significant correlation with the equatorial Pacific. Moreover, both observations and GOGA-SAML show a positive correlation with SST anomalies off Brazil, meaning that warmer air temperature over SESA is related to a warmer neighboring ocean. These SST anomalies off Brazil do not force directly the temperature over SESA. Instead, by experimental design they are a response to the ENSO forcing (see also Sect. 4). Thus, the high predictability in fall originates in the Pacific ocean, and as the south Atlantic responds to ENSO, the air–sea coupling changes the evolution of the ENSO signal in SESA. Note that the simulated SST anomalies off Brazil are weaker than the observed ones (compare panels of Fig. 4), mainly because we are taking the ensemble mean of the experiments, and also because we may be missing important oceanic mechanisms for the creation of the anomalies due to the use of a slab ocean.

To further understand the role of the ocean off Brazil and determine its influence during fall before and after the peak of ENSO we proceed as follows. We first construct the normalized Niño3.4 index in December–January and consider it as representative of the ENSO behavior (e.g., Barreiro and Tippmann 2008). We then perform a regression analysis of the fields onto this index to examine the anomalies related to ENSO during MJJ0 (development phase) and MJJ+ (decay phase).

The regression analysis reveals that the largest anomalies and maximum predictability of surface temperature in MJJ in PERIOD1 occur during year 0 of ENSO, that is, while it is growing (Fig. 5). The regression maps also show a large eastern Pacific temperature anomaly in MJJ0, whereas in MJJ+ the equatorial anomaly has almost disappeared. This agrees with the literature, showing that during this period ENSO started early in the year and had largely decayed before fall of the following year (though the maps of Fig. 5 show surface air temperature they are highly correlated to SST in the tropics). The ENSO signal over SESA during MJJ0 is seen both in observations and in the model simulations, and is very robust. Nevertheless, while in observations the warming is restricted to SESA, the simulated warming covers a large portion of tropical South America (upper panels of Fig. 5). The correlation between observed and simulated temperature over SESA during MJJ0 is 0.73 for GOGA-SAML and 0.67 for GOGA-SACL, thus suggesting that air–sea interaction does not play a fundamental role.

During the MJJ+ years of PERIOD1 the correlation between observed and simulated surface air temperature is 0.55 for GOGA-SAML (significant at 5% level) but only 0.24 for GOGA-SACL. Thus, the improvement in predictability (compared to GOGA-SACL) seen in the upper

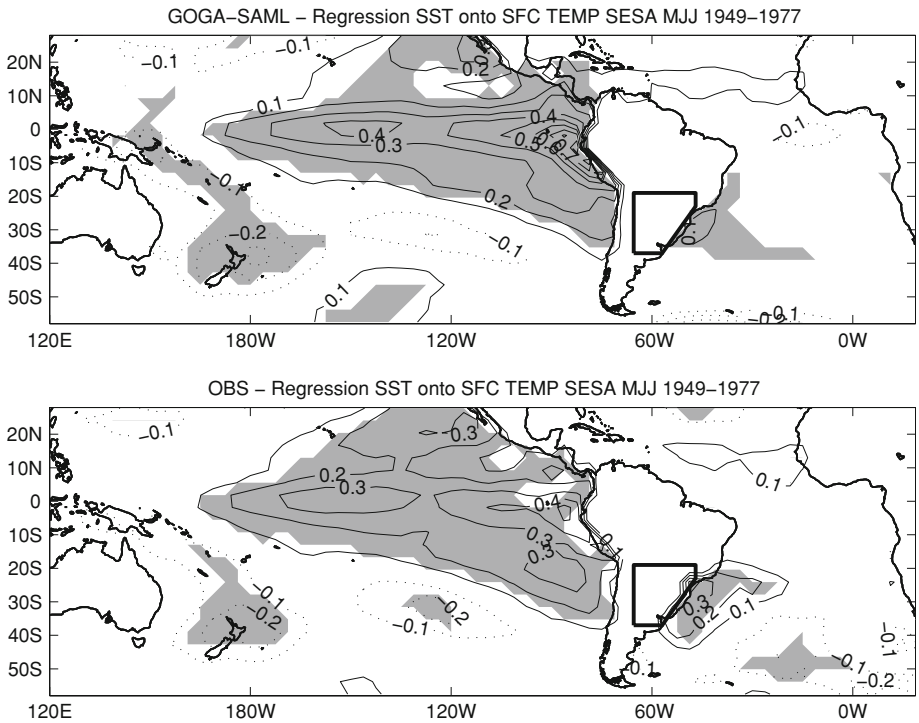

Fig. 4 Regression of SST (K) onto the evolution of surface temperature in SESA in MJJ season. *Upper panel* shows for GOGA-SAML, and *lower panel* for observations. *Shading* indicates statistical significance at the 5% level using a 2-sided student *t* test. The *box* marks the SESA region

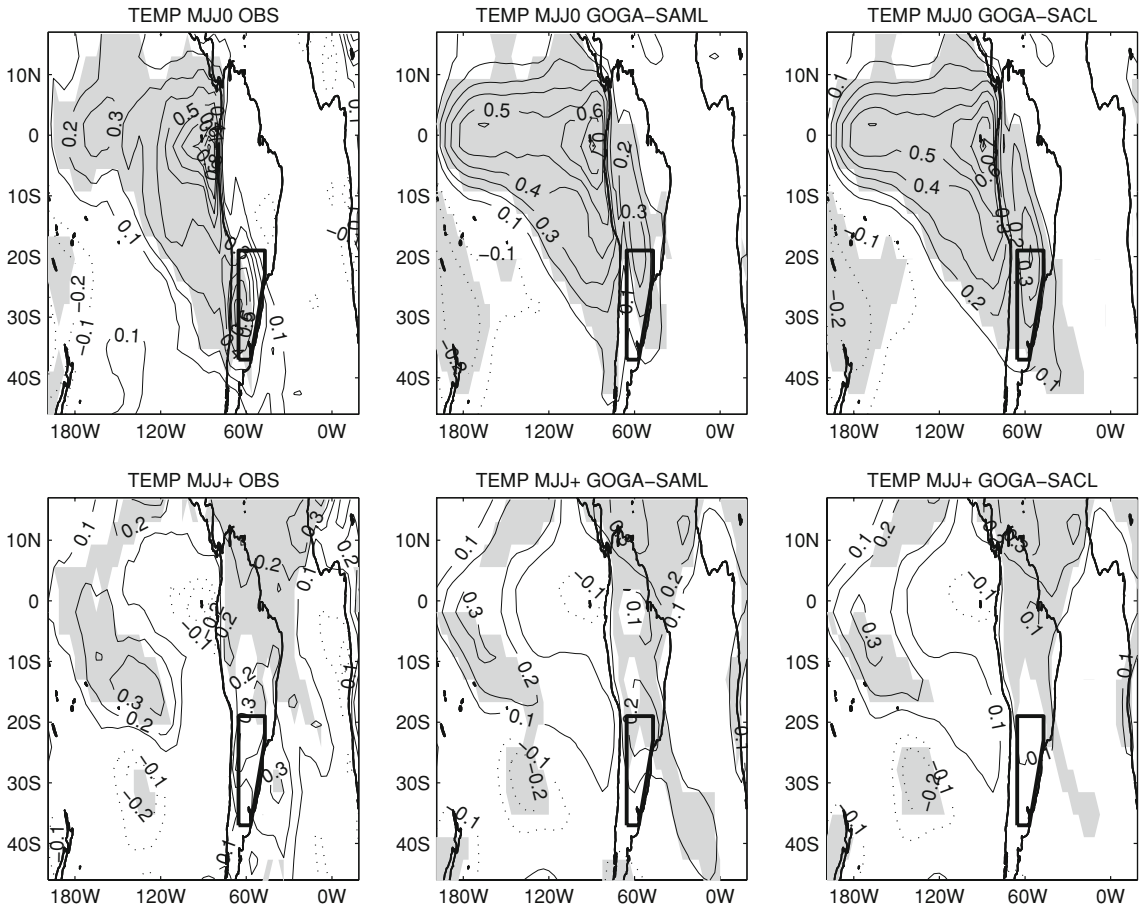

Fig. 5 Regression of surface air temperature (K) onto the normalized Niño3.4 DJ index for the period 1949–1977 for observations (*left*) and experiments GOGA-SAML (*middle*) and GOGA-SACL (*right*). *Upper panels* show season MJJ0, and *lower panels* show season MJJ+. *Shading* and *box* as in Fig. 4

panel of Fig. 2 during the MJJ season occurs mainly in MJJ+, that is when ENSO is decaying. According to the regression analysis the south Atlantic tends to warm up during El Niño years as result of changes in the surface heat fluxes induced through atmospheric teleconnections (see also Sect. 4). Comparison between the maps for GOGA-SACL and GOGA-SAML (lower panels of Fig. 5) shows that the air–sea interaction in the south Atlantic strengthens the ENSO signal over the ocean and SESA, resulting in simulated anomalies that are closer to observations.

In PERIOD2 the model shows lower predictability in MJJ, concordant with a decrease in ENSO influence (lower panel Fig. 2). Moreover, the inclusion of the slab ocean degrades the model performance in this season. The correlation between observed and simulated temperature in SESA for MJJ0 years is 0.69 for GOGA-SAML and 0.57 for GOGA-SACL, suggesting that the air–sea coupling is working to help the model to simulate the right response. Note that the model captures very well the warming in SESA and neighboring south Atlantic, and does not warm tropical South America as in PERIOD1 (upper panels of Fig. 6). This may have to do with the existence of a cold anomaly in the equatorial Atlantic that opposes the El Niño warming. On the other hand, for MJJ+ years the correlation decreases to 0.25 for GOGA-SAML and to 0.5 for GOGA-SACL. This latter result has to do with the slow decay of ENSO. Contrary to PERIOD1, in this latter period the SST anomaly in MJJ+ is still very large in the eastern Pacific and the model responds very strongly to it as shown in the regression maps (lower panels of Fig. 6). While in observations there is no significant warming over SESA, experiment GOGA-SACL shows an already too strong warming in this region that is further strengthened by air–sea coupling in GOGA-SAML, resulting in a wrong response. This leads to the lower predictability skill seen in the lower panel of Fig. 2 when the slab ocean is used.

Thus, in both periods the local air–sea interaction strengthens the remote ENSO signal. This may result in an increase/decrease of the model skill depending on how well simulated are the direct ENSO-induced anomalies.

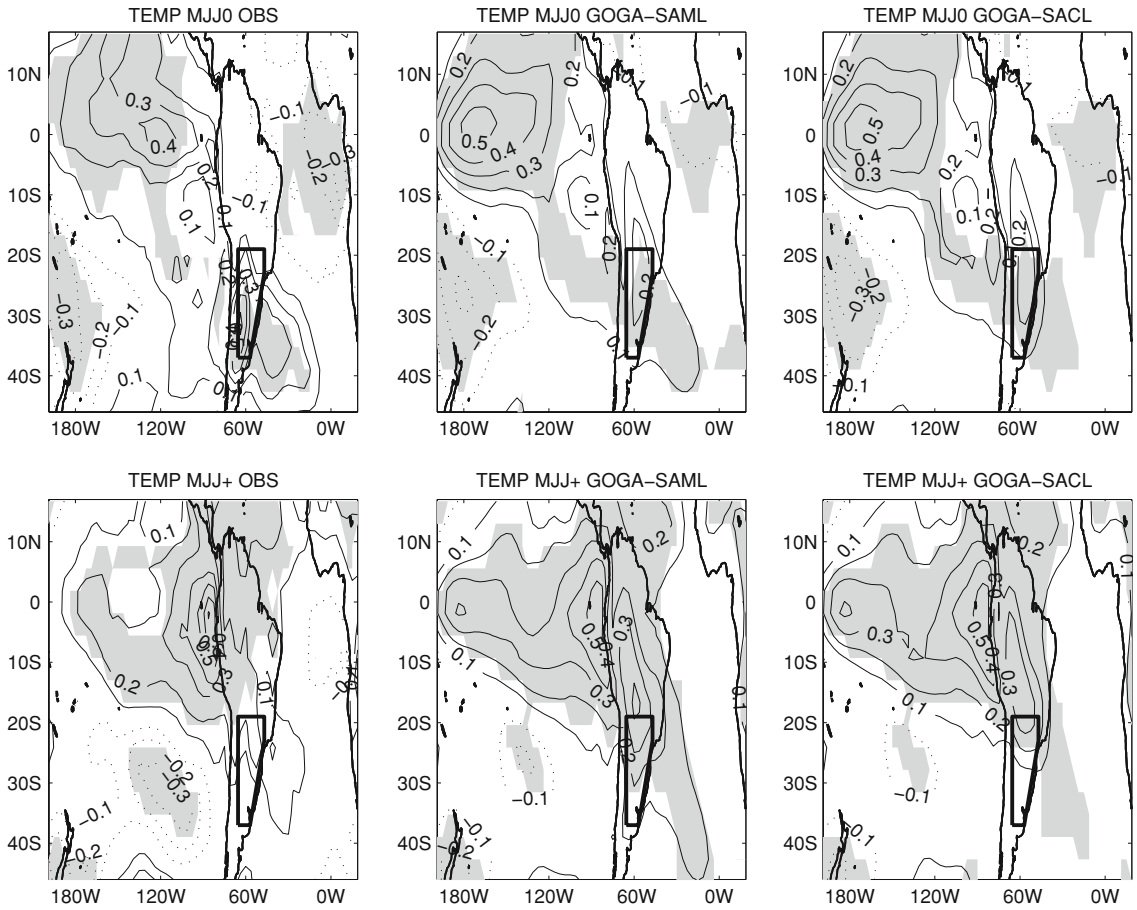

Fig. 6 Same as Fig. 5, but for period 1978–2006

4 Role of thermodynamic coupling

During PERIOD1 the skill of the model coupled to a slab ocean in the south Atlantic (GOGA-SAML) is significantly larger than when imposing climatological SST in that region (GOGA-SACL). Moreover, we show in Sect. 3.2 that during MJJ the local coupling strengthens the ENSO signal over the neighboring land. On the other hand, overall the skill is largest when the model is forced with historical SST anomalies everywhere (GOGA experiment). It is thus not clear if the strengthening and increase in skill is due to the direct impact on SESA of the ENSO-induced SST anomaly off Brazil, or if it suggests a role for a two-way air–sea coupling that modulates the direct ENSO influence.

We note that while GOGA has perfect SST anomalies, GOGA-SAML creates the SST anomalies using a slab ocean that may be missing important oceanic mechanisms. Thus, the comparison between GOGA and GOGA-SAML may not be the best way to identify the role of the thermodynamic interaction. To address this issue we performed another GOGA-type experiment with historical SST everywhere except in the south Atlantic where we specify the ensemble mean SST of the GOGA-SAML experiment. The difference in skill between GOGA-SAML and this new run (GOGA-SAML-NOC) will be due to the local air–sea coupling in the south Atlantic.

Figure 7 shows the predictability skill of the model for surface temperature in PERIOD1. (In PERIOD2 the skill is relatively low and significant only during winter and is not studied further here.) The new experiment is more skillful than GOGA-SACL showing that the ENSO-induced SST anomalies off Brazil help to represent correctly the surface temperature anomalies over SESA, in the absence of active coupling. Moreover, except for MAM, allowing active thermodynamic coupling in the south Atlantic consistently increases the predictability of the model for most of the year, particularly since late fall to early spring. Thus, two-way air–sea interaction plays a role in improving the model's skill in representing surface temperature anomalies over SESA in this period.

To further study the effect of the air–sea coupling in the south Atlantic we look at the changes in the evolution of anomalies over SESA. As a first step we compared the persistence of seasonal temperature anomalies over SESA

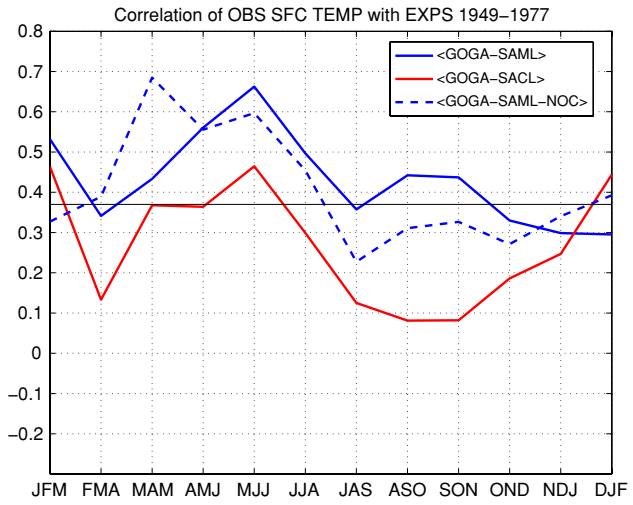

Fig. 7 Same as Fig. 2, for experiments GOGA-SAML, GOGA-SACL, and GOGA-SAML-NOC. This last experiment has historical SST anomalies everywhere except in the south Atlantic where it has prescribed the ensemble mean SST anomalies of the GOGA-SAML experiment

for the experiments GOGA-SACL and GOGA-SAML (Fig. 8). This figure shows that the air–sea interaction in the south Atlantic increases the persistence of the air temperature anomalies, particularly during fall. Since we are taking the ensemble mean these plots show the persistence of temperature anomalies forced by tropical Pacific SST.

Moreover, during ENSO events the turbulent surface heat flux anomalies over the oceanic region off Brazil in GOGA-SAML are significantly smaller than those of GOGA-SACL (Fig. 9). The figure shows that net heat flux anomalies are positive and large as ENSO develops, then become close to zero and even negative during high summer, and become positive again in MAM (Fig. 9e). As expected for a slab ocean, the SST warming lags the surface fluxes by about one season (Fig. 9f). Overall, latent heat flux anomalies dominate during the whole event, while sensible heat flux, shortwave radiation and longwave radiation are smaller and of similar magnitude. This is particularly true for the GOGA-SACL experiment. When air–sea interaction is allowed in the south Atlantic the anomalies of the turbulent fluxes decrease substantially, while the radiation fluxes remain mostly unchanged. The latent heat anomaly in GOGA-SAML decreases by a factor of two at the beginning and end of the ENSO event (including MJJ0 and MJJ+) compared to that in GOGA-SACL, so that the magnitude of the latent heat anomalies become comparable to those of the longwave radiation and of the sensible heat.

The increase in the persistence of atmospheric anomalies and the decreased turbulent heat flux anomalies when air–sea interaction is allowed is consistent with the thermodynamic feedback proposed by Barsugli and Battisti (1998) and Saravanan and McWilliams (1998). The process can be summarized as follows: the ocean response to an atmospheric temperature anomaly (due to ENSO) decreases the air–sea temperature difference which in turn results in decreased turbulent heat fluxes and reduced effective damping of the original atmospheric anomaly.

5 Precipitation

5.1 Predictability

Figure 10 shows the correlation skill for precipitation in several model configurations. Again, as in the case of air temperature, the model shows no skill in simulating the observed variability of precipitation when forced with only Atlantic SST anomalies, independently of the season. In fact, for many seasons the correlation with observed

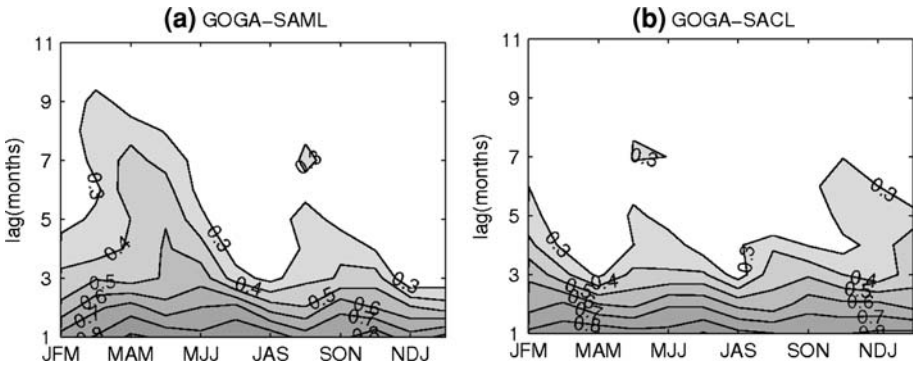

Fig. 8 Persistence of surface temperature anomalies over SESA for different trimesters calculated as the autocorrelation over the period 1949–2006 for (**a**) GOGA-SAML, (**b**) GOGA-SACL. Values larger than 0.3 are statistically significant at the 5% level using a two-sided student *t* test. Note the large increase in persistence during late summer and fall when air–sea coupling is allowed in the south Atlantic

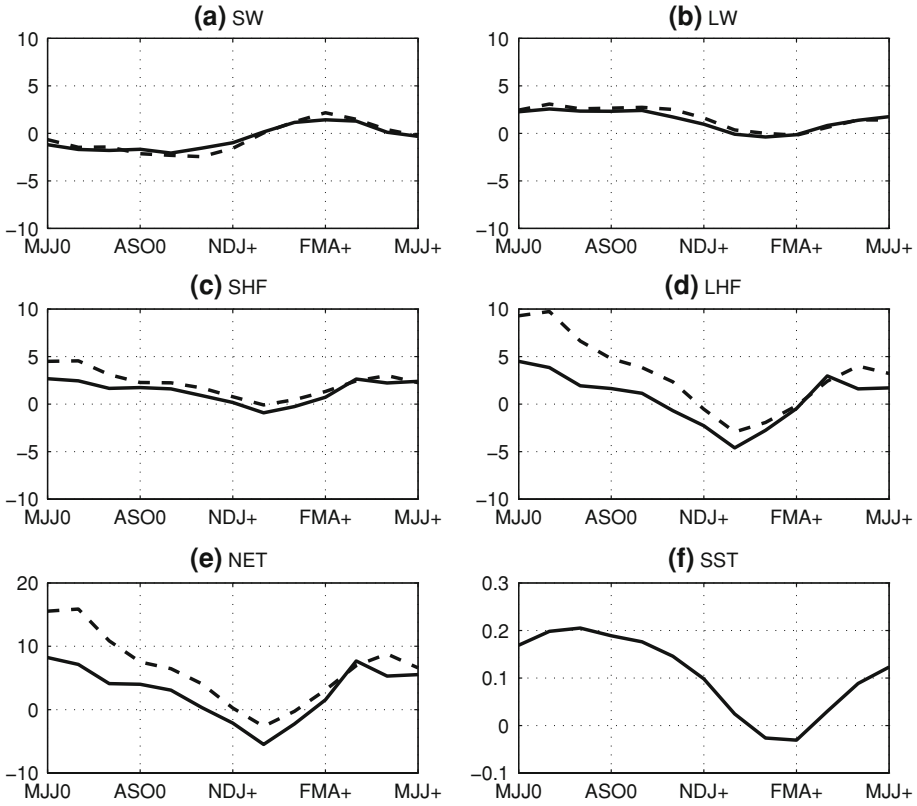

Fig. 9 Evolution of surface heat flux (W m^{-2}) and SST anomalies (K) in the oceanic region off Brazil defined by the box [55°W–30°W, 37°S–19°S]. The panels show the regression onto normalized Niño3.4 DJ for several seasons before and after the peak of ENSO calculated over the period 1949–2006 of (**a**) shortwave radiation, (**b**) longwave radiation, (**c**) sensible heat flux, (**d**) latent heat flux, (**e**) net surface flux, and (**f**) SST anomalies. The *solid line* is for experiment GOGA-SAML, and the *dashed line* is for experiment GOGA-SACL. In panel (**f**) only the SST for GOGA-SAML is shown because GOGA-SACL has climatological SST prescribed in the south Atlantic

precipitation is negative (although not significant) suggesting that imposing SST in this basin tends to induce precipitation anomalies of different sign from the observed.

Also, it can be seen that the predictability of precipitation strongly depends on the period considered. The two periods (1949–1977 and 1978–2006) show large predictability during spring, the most robust ENSO signal over SESA (e.g., Grimm et al. 2000; Nobre et al. 2006). During this season the correlation between Niño3.4 and observed precipitation is close to or higher than 0.7 for both periods, suggesting that ENSO can explain about 50% of the rainfall variability in the region. We note that in PERIOD1 the skill of GOGA during spring is significantly lower than that of GOGA-SACL. This may be related to a wrong response of the model to south Atlantic SST, supported by the fact that AOGA has negative skill particularly in season OND, as mentioned before.

In addition to the spring predictability maximum, in PERIOD2 there is increased predictability during summertime, and a second maximum of predictability in late fall and early winter that is absent in PERIOD1. Interestingly, this new maximum is as high as the spring one and depends also on the ENSO signal as shown by the observed correlation between rainfall over SESA and Niño3.4 index (lower panel Fig. 10). (Figure 3 confirms that the observed correlation is independent on the ENSO index considered.) Note, however, that in late fall the simulated correlation is higher than the observed correlation with Niño3.4, in opposition to the spring season. This suggests a relatively weak ENSO signal embedded in large internal atmospheric variability that the averaging process performed to obtain the ensemble mean is able to bring forward.

During the spring season of PERIOD1 the use of climatological SST in the south Atlantic results in higher predictability than when using a slab ocean in this region. We argue that at least part of this is related to the use of a time independent mixed layer depth of 50 m, that represents an average depth over the year. Since in winter and spring the mixed layer in the south Atlantic reaches depths larger than 100 m (Kara et al. 2003) the used depth may not be suitable for these seasons. To test this hypothesis we run another (10-member ensemble) experiment identical to GOGA-SAML but with a 100 m deep slab ocean in the south Atlantic. As the other experiments this new run has no skill in the first part of the year of PERIOD1, but increases significantly during spring, resulting in correlation values that are comparable to those of GOGA-SACL (Fig. 11). Moreover, over the whole period 1949–2006 we find that the predictability of precipitation in the run with a 100 m deep slab ocean is lower than that of GOGA-SAML in summer and fall and higher in winter and spring, agreeing with the seasonal evolution of the mixed layer depth (Fig. 12). (We note that for temperature the use of a 100 m deep slab ocean does not significantly change the

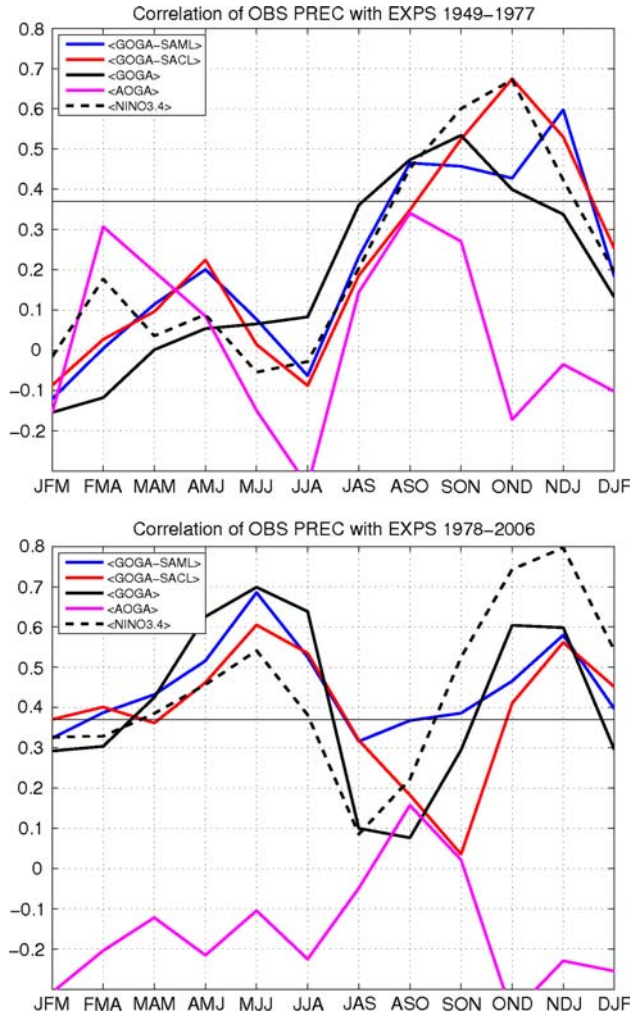

Fig. 10 Same as Fig. 2, but for precipitation

correlation skill.) The sensitivity shown by the precipitation stresses the importance of simulating correctly the ocean mixed layer in order to better represent the air–sea thermodynamic interaction (see also Saravanan and Chang 1999).

During PERIOD 2 the skill of GOGA-SAML is higher than that of GOGA-SACL during most of the seasons, showing that the use of a slab ocean in the south Atlantic can also improve the model's ability to reproduce rainfall anomalies (lower panel, Fig. 10). However, GOGA caps the skill during most of the year, with the exception of late winter-early spring, where GOGA-SAML has larger (but barely significant) skill. To further study the role of the air–sea interaction in the south Atlantic we computed the correlation skill of the experiment GOGA-SAML-NOC, where the SST anomalies generated in GOGA-SAML are imposed in the south Atlantic. As shown in Fig. 13, the largest improvement over GOGA-SACL is mainly during fall and early winter. Furthermore, the new experiment has even higher skill than GOGA-SAML during fall, and is

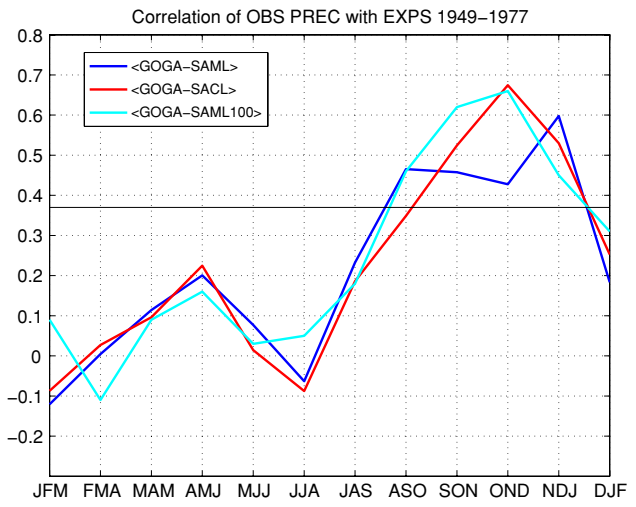

Fig. 11 Dependence of the predictability of precipitation on the depth of the slab ocean used in the south Atlantic for the period 1949–1977. GOGA-SAML100 is an experiment analogous to GOGA-SAML but with a 100 m deep slab ocean. The *horizontal line* as in Fig. 2

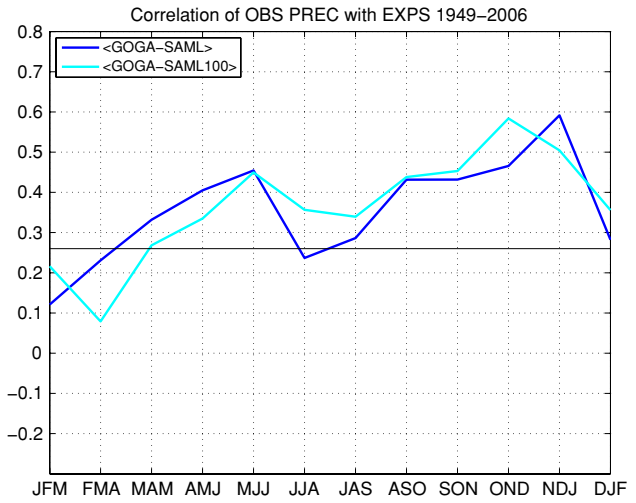

Fig. 12 Dependence of the predictability of precipitation on the depth of the slab ocean used in the south Atlantic for the period 1949–2006. The *horizontal line* marks the values significant at 5% level using a 2-sided student *t* test

similar to that of the GOGA experiment. This suggests that a responsive ocean off Brazil tends to increase the skill compared to the use of climatology, but a local two-way thermodynamic coupling is not necessary to reproduce rainfall anomalies over SESA during this season.

5.2 Fall season

We found that the most robust signal in SESA is the ENSO influence on rainfall during the springtime, in agreement with the literature. We do not focus on this season because

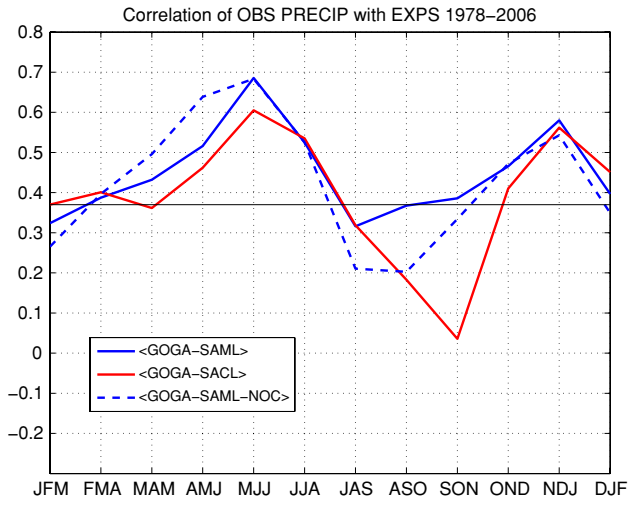

Fig. 13 Same as Fig. 7 but for precipitation during PERIOD2

it has been studied extensively (e.g., Nobre et al. 2006 and references therein). Instead, as for surface temperature we focus on fall, a season that according to Sect. 5.1 is influenced by ENSO only after the mid-1970s (PERIOD2). Even though during PERIOD2 the maximum of rainfall predictability occurs in MJJ (lower panel Fig. 10), we consider AMJ because the observed signal is larger (results are similar for season MJJ). In this season the use of a slab ocean in the south Atlantic slightly increases the skill of the model, but it is still significantly smaller than in the GOGA experiment.

As for the surface temperature, we regress fields onto Niño3.4 to examine the anomalies related to ENSO during AMJ0 (development phase) and AMJ+ (decay phase). The regression analysis shows that there are no precipitation anomalies during AMJ0 over SESA in the observations or in the model simulations, suggesting that ENSO has no influence (not shown). On the other hand, in AMJ+ there are large observed positive anomalies in the northeastern region of SESA associated with warm ENSO events (upper left panel, Fig. 14). This influence was recently reported in the observational work of Antico (2008) and is consistent with the observed changes in ENSO evolution after the mid-1970s. As shown by Antico (2008) the observed precipitation anomalies are accompanied by enhanced low-level northwesterly winds that transport moisture into the region (Fig. 14). Moreover, the rainfall anomalies tend to coincide with a region of low-level convergence in the northeastern part of SESA.

The model simulations also capture the ENSO influence with increased rainfall in SESA accompanied by enhanced northerly moisture fluxes, but locate the maximum rainfall anomalies in the northwestern corner of SESA evidencing the model bias mentioned in Sect. 2 (Fig. 14). Also, rainfall in the model tends to occur in regions of low-level moisture convergence. However, the maximum simulated convergence is located in the northwestern corner of SESA, where observations show only a weak (non-significant) convergence. Allowing the ocean off Brazil to respond tends to reduce the moisture convergence and thus precipitation in the northwestern corner of SESA as well as to increase moisture convergence off the Brazilian coast at about 25°S, resulting in anomalies that are closer to observations (lower panels of Fig. 14). The regression maps for GOGA-SAML-NOC are very similar to those of GOGA-SACL and are not shown. Nevertheless, while the correlation between observed and simulated precipitation over SESA during AMJ+ is about 0.7 for GOGA-SAML and GOGA-SACL, it is 0.86 for GOGA-SAML-NOC showing that this latter run captures better the ENSO influence in this season, thus resulting in the higher skill shown in Fig. 13.

6 Summary and discussion

This study investigates the predictability of climate over Southeastern South America with particular emphasis on the role of the south Atlantic and on the inter-decadal changes in predictability. We perform tailored model experiments using an AGCM either in stand-alone mode or coupled to a slab ocean in the south Atlantic that takes into account the thermodynamic interaction between the ocean and the atmosphere. We calculate predictability as the linear correlation between the observed field and the simulated ensemble mean of precipitation and surface air temperature.

Results suggest that the south Atlantic does not directly influence the temperature or precipitation over SESA, as shown by the experiment forced with only Atlantic SST anomalies (AOGA). This agrees with previous studies that focused on particular seasons (e.g., Barreiro et al. 2002; Robertson et al. 2003). Moreover, in our model the skill of the simulation can even decrease when Atlantic SST anomalies are imposed as shown by the comparison of the predictability of precipitation of the GOGA experiment versus that of GOGA-SACL in the spring season during period 1949–1977.

In the model the predictability of climate over SESA comes mainly from the Pacific ocean, in agreement with the literature (e.g., Nobre et al. 2006). Moreover, the predictability of temperature and precipitation was found to show large inter-decadal variability mainly due to changes in the ENSO signal: the model shows relatively high predictability when ENSO influences SESA and very low predictability when it does not. As result, during the period 1949–1977 temperature shows high predictability during late fall and early winter, while precipitation shows high

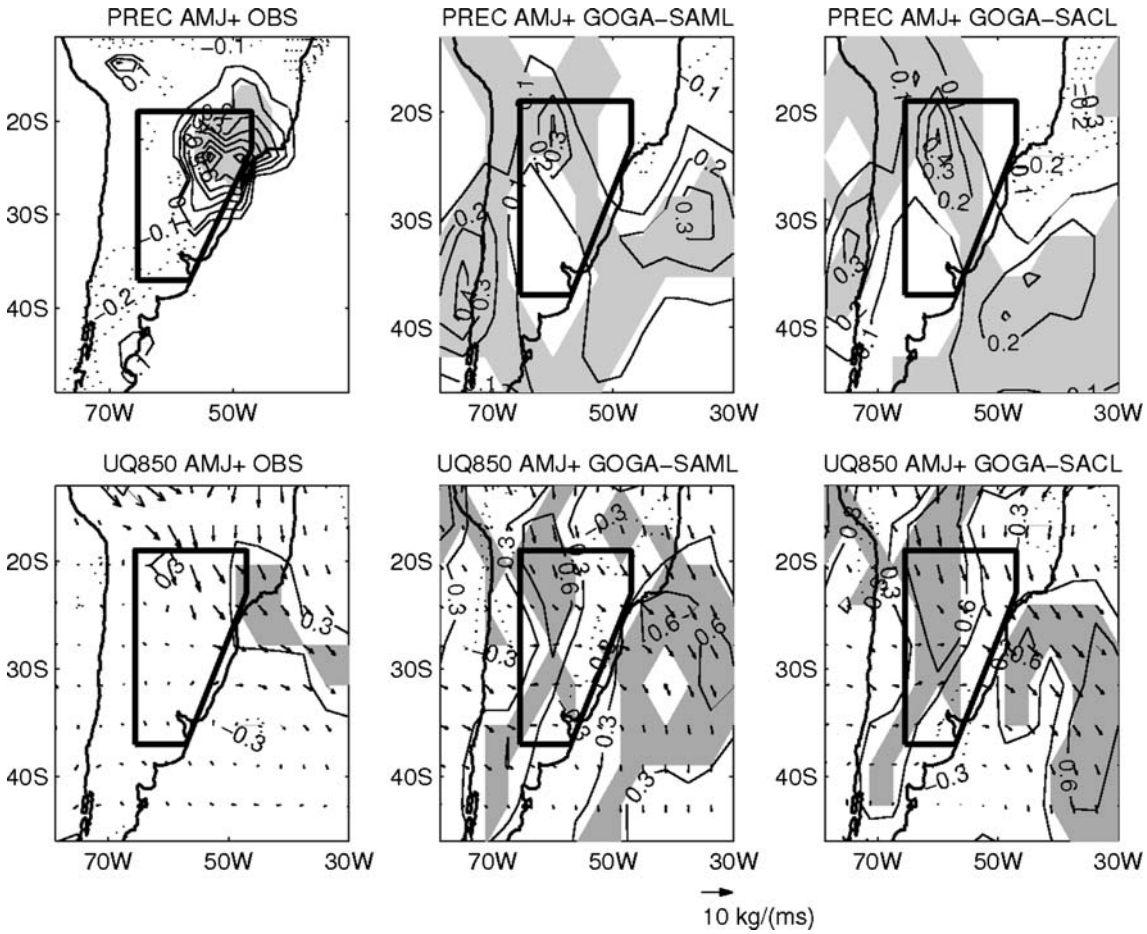

Fig. 14 Regression maps in season AMJ+ onto normalized Niño3.4 DJ index for observations (*left*), GOGA-SAML (*middle*) and GOGA-SACL (*right*) during period 1978–2006. *Upper panels* show rainfall (mm day^{-1}), and *lower panels* show the 850 hPa moisture fluxes. *Shading* in *upper panels* marks the regions where precipitation is significant at the 5% level. In the *lower panels* contours indicate correlation between 850 hPa moisture convergence and the Niño3.4 DJ index while the *shading* marks the regions where the correlation is significant at the 10% level using a two-sided student *t* test

predictability only during spring. In the second period 1978–2006 the predictability of temperature decreases particularly during fall so that the maximum is now in the winter season. On the other hand, in this latter period precipitation shows high predictability not only in spring but also during late fall. These changes arise due to the persistence of ENSO anomalies up to season MJJ+ in the decaying phase, as suggested in the observational work of Antico (2008).

We note that the linear analysis used in this work does not allow to study separately the influence of El Niño versus that of La Niña events. This may be of particular importance as it has been previously reported that warm and cold ENSO events do not affect SESA in exactly opposite ways (Nobre et al. 2004). Nonetheless, the linear analysis is robust, allows easy interpretation, and gives an average measure of the response of the climate to Pacific anomalies.

Moreover, we show for the first time that the south Atlantic can play a secondary role in affecting climate anomalies over SESA through modifying the ENSO remote signal. We found that the ocean off Brazil and Uruguay responds to the ENSO signal by warming (cooling) during warm (cold) ENSO events through changes in the surface heat fluxes. This oceanic warming in turn alters the evolution of the atmospheric anomalies through a local thermodynamic feedback, resulting in an increased persistence of the original atmospheric disturbance. A similar result was found for the northern hemisphere mid-latitude region during wintertime (Alexander et al. 2002). We found that the effect is largest for the temperature and is able to increase the skill of the AGCM when coupled to a slab ocean. The thermodynamic feedback can also degrade the skill of the model if the air–sea interaction operates over an initially wrong anomaly. This is, for example, the case of fall MJJ+ temperature during 1978–2006, and stresses the

fact that a good prediction will result from the right simulation of both the remote influence as well as of the local feedbacks.

For precipitation we found that allowing air–sea interaction in the south Atlantic can also lead to a small increase in skill due to the response of the ocean to the ENSO forcing. However, for seasons with relatively high predictability we found no evidence that active coupling increases the skill (Fig. 13).

Overall, our results show that the predictability of precipitation is larger than that of surface air temperature. This is again tied to the largest effect of ENSO on precipitation seen by the large correlations, particularly during spring, and is in agreement with the literature. As mentioned in the introduction Barros et al. (2002) suggest that the weak ENSO influence on surface temperature is due to the canceling effect of opposing processes: for example, an increased northerly flow will tend to warm SESA by advecting heat from the tropics, and at the same time it will tend to cool SESA by advecting moisture due to the increase in cloud cover and evaporation that are associated with enhanced rainfall.

Moreover, our results suggest that whenever ENSO influences temperature it does not influence rainfall, and vice versa (compare Figs. 2, 10). Thus, the seasonal predictability of each variable tends to be out of phase. For example, during 1978–2006 the predictability of precipitation is largest in fall and spring, while the predictability of temperature is largest in winter. During this period the decrease in ENSO influence on temperature in fall (compared to PERIOD1) is concordant with an increase in ENSO influence on precipitation. We showed this is accompanied by an anomalous northerly flow (Fig. 14) and thus, it seems to agree with the hypothesis of Barros et al. (2002). On the other hand, during fall of period 1949–1977 ENSO influences the temperature, but not the precipitation, and is not accompanied by significant low level flow anomalies (not shown). More research is necessary to further elucidate the ENSO influence on climate anomalies over SESA and understand the predictability of the different fields.

Finally, it should be noted that the model used in this study has low resolution and shows significant biases in representing rainfall. Thus, the results presented here should be further tested using other climate models. In particular, the use of high resolution coupled atmosphere–ocean models would help to further understand the processes involved in the air–sea interaction in the south Atlantic and its impact over SESA. Moreover, even though the surface heat fluxes govern a significant portion of the SST evolution, wind stress and oceanic processes may be also important in determining the SST in the south Atlantic, thus further modifying the impact of the ocean on the atmosphere.

Acknowledgments The author would like to thank M. Renom for useful discussions during the course of the study, and to A. Cherchi for commenting on a first version of the manuscript. We also thank two anonymous reviewers for their suggestions that greatly improved the original manuscript. The research leading to these results has received funding from the Programa de Desarrollo Tecnológico in Uruguay, and the European Community's Seventh Framework Programme (FP7/2007-2013) under Grant Agreement No 212492.

References

Alexander M, Blade AI, Newman M, Lanzante JR, Lau N-C, Scott JD (2002) The atmospheric bridge: the influence of ENSO teleconnections on air–sea interaction over the global oceans. J Clim 15:2205–2231

Antico PL (2008) Relationships between autumn precipitation anomalies in southeastern South America and El Niño event classification. Int J Climatol. doi:10.1002/joc.1734

Barreiro M, Tippmann A (2008) Atlantic modulation of El Niño influence on summertime rainfall over Southeastern South America. Geophys Res Lett 35:L16704. doi:10.1029/2008GL035019

Barreiro M, Chang P, Saravanan R (2002) Variability of the South Atlantic Convergence Zone as simulated by an atmospheric general circulation model. J Clim 15:745–763

Barreiro M, Chang P, Saravanan R (2005) Simulated precipitation response to SST forcing and potential predictability in the region of the South Atlantic Convergence Zone. Clim Dyn 24:105–114. doi:10.1007/s00382-004-0487-9

Barros VR, Silvestri G (2002) The relationship between sea surface temperature at the subtropical south central Pacific and precipitation in southeastern South America. J Clim 15:251–267

Barros VR, Grimm AM, Doyle ME (2002) Relationship between temperature and circulation in southeastern South America and its influence from El Niño and La Niña events. J Meteo Soc Japan 80:21–32

Barsugli JJ, Battisti DS (1998) The basic effects of atmosphere-ocean thermal coupling on midlatitude variability. J Atmos Sci 55:477–493

Camilloni I, Barros V (2003) Extreme discharge events in the Parana River and their climate forcing. J Hydrol 278:94–106

Chan SC, Behera SK, Yamagata T (2008) Indian Ocean Dipole influence on South American rainfall. Geophys Res Lett 35, L14S12. doi:10.1029/2008GL034204

Chaves RR, Nobre P (2004) Interactions between sea surface temperature over the South Atlantic Ocean and the South Atlantic Convergence Zone. Geophys Res Lett 31:L03204. doi:10.1029/2003GL018647

Chen M, Xie P, Janowiak JE, Arkin PA (2002) Global land precipitation: a 50-yr monthly analysis based on gauge observations. J Hydrometeorol 3:249–266

Chiang JCH, Sobel AH (2002) Tropical tropospheric temperature variations caused by ENSO and their influence on the remote tropical climate. J Clim 15:2616–2631

Diaz AF, Studzinski CD, Mechoso CR (1998) Relationships between precipitation anomalies in Uruguay and southern Brazil and sea surface temperature in the Pacific and Atlantic Oceans. J Clim 11:251–271

Doyle ME, Barros VR (2002) Midsummer low-level circulation and precipitation in subtropical South America related sea surface

temperature anomalies in the South Atlantic. J Clim 15:3394–3410

Grimm AM, Barros VR, Doyle ME (2000) Climate variability in Southern South America associated with El Niño and La Niña events. J Clim 13:35–58

Kalnay E, Kanamitsu M, Kistler R, Collins W, Deaven D, Gandin L, Iredell M, Saha S, White G, Woollen J, Zhu Y, Leetmaa A, Reynolds B, Chelliah M, Ebisuzaki W, Higgins W, Janowiak J, Mo KC, Ropelewski C, Wang J, Jenne R, Joseph D (1996) The NCEP/NCAR 40-year reanalysis project. Bull Am Meteorol Soc 77:437–471

Kara AB, Rochford PA, Hurlburt HE (2003) Mixed layer depth variability over the global ocean. J Geophys Res 108(C3). doi:10.1029/2000JC000736

Kiladis GN, Diaz HF (1989) Global climatic anomalies associated with extremes in the Southern Oscillation. J Clim 2:1069–1090

Kucharski F, Molteni F, Bracco A (2005) Decadal interactions between the western tropical Pacific and the North Atlantic Oscillation. Clim Dyn. doi:10.1007/s00382-005-0085-5

Molteni F (2003) Atmospheric simulations using a GCM with simplified physical parametrizations. I. Model climatology and variability in multi-decadal experiments. Clim Dyn 20:175–191

Nobre P, Marengo J, Cavalcanti IAF, Obregon G, Barros V, Camilloni I, Campos N, Ferreira AG (2004) Seasonal-to-decadal predictability and prediction of South American climate. White paper CLIVAR Workshop on Atlantic Predictability, Reading, UK

Nobre P, Marengo JA, Calvacanti IAF, Obregón G, Barros V, Camilloni I, Campos N, Ferreira AG (2006) Seasonal-to-decadal predictability and prediction of South American climate. J Clim 19:5988–6004

Robertson AW, Mechoso CR (2000) Interannual and interdecadal variability of the South Atlantic Convergence Zone. Mon Weather Rev 128:2947–2957

Robertson AW, Farrara JD, Mechoso CR (2003) Simulations of the atmospheric response to South Atlantic sea surface temperature anomalies. J Clim 16:2540–2551

Ropelewski CH, Halpert S (1987) Global and regional scale precipitation patterns associated with the El Niño-Southern Oscillation. Mon Weather Rev 115:1606–1626

Ropelewski CH, Halpert S (1989) Precipitation patterns associated with the high index phase of the Southern Oscillation. J Clim 2:268–284

Saji NH, Ambrizzi T, Ferraz SET (2005) Indian Ocean Dipole mode events and austral surface air temperature anomalies. Dyn Atmos Oceans 39:87–101

Saravanan R, McWilliams JC (1998) Advective ocean-atmosphere interaction: an analytical stochastic model with implications for decadal variability. J Clim 11:168–188

Saravanan R, Chang P (1999) Oceanic mixed layer feedback and tropical Atlantic variability. Geophys Res Lett 26(24):3629–3632

Silvestri GE (2004) El Niño signal variability in the precipitation over southeastern South America during austral summer. Geophys Res Lett 31. doi:10.1029/2004GL020590

Smith TM, Reynolds RW (2004) Improved extended reconstruction of SST (1854–1997). J Clim 17:2466–2477

Taschetto AS, Wainer I (2008) Reproducibility of South American precipitation due to subtropical South Atlantic SSTs. J Clim 21(12):2835–2851

Vianna Cuadra S, Porfirio Da Rocha R (2007) Sensitivity of regional climatic simulation over Southeastern South America to SST specification during austral summer. Int J Climatol 6:793–804

Wang B (1995) Interdecadal changes in El Niño onset in the last four decades. J Clim 8:267–285

Wolter K, Timlin MS (1993) Monitoring ENSO in COADS with a seasonally adjusted principal component index. In: Proceedings of the 17th Climate Diagnostics Workshop, Norman, OK, NOAA/NMC/CAC, NSSL, Oklahoma Climate Survey, CIMMS and the School of Meteorology, University of Oklahoma, pp 52–57

Wolter K, Timlin MS (1998) Measuring the strength of ENSO events—how does 1997/98 rank? Weather 53:315–324

Yulaeva E, Wallace JM (1994) The signature of ENSO in global temperature and precipitation fields derived from the Microwave Sounding Unit. J Clim 7:1719–1736